Title
KCNE2 forms potassium channels with KCNA3 and KCNQ1 in the choroid plexus epithelium

Journal
The FASEB Journal, 25(12)

ISSN
0892-6638

Authors
Roepke, Torsten K
Kanda, Vikram A
Purtell, Kerry
et al.

Publication Date
2011-12-01

DOI
10.1096/fj.11-187609

KCNE2 forms potassium channels with KCNA3 and KCNQ1 in the choroid plexus epithelium

Torsten K. Roepke,*,†,[1] Vikram A. Kanda,* Kerry Purtell,* Elizabeth C. King,*,† Daniel J. Lerner,†,[2] and Geoffrey W. Abbott*,†,[3]

*Department of Pharmacology and †Department of Medicine, Weill Medical College of Cornell University, New York, New York, USA

ABSTRACT **Cerebrospinal fluid (CSF) is crucial for normal function and mechanical protection of the CNS. The choroid plexus epithelium (CPe) is primarily responsible for secreting CSF and regulating its composition by mechanisms currently not fully understood. Previously, the heteromeric KCNQ1-KCNE2 K^+ channel was functionally linked to epithelial processes including gastric acid secretion and thyroid hormone biosynthesis. Here, using *Kcne2*$^{-/-}$ tissue as a negative control, we found cerebral expression of KCNE2 to be markedly enriched in the CPe apical membrane, where we also discovered expression of KCNQ1. Targeted *Kcne2* gene deletion in C57B6 mice increased CPe outward K^+ current 2-fold. The *Kcne2* deletion-enhanced portion of the current was inhibited by XE991 (10 μM) and margatoxin (10 μM) but not by dendrotoxin (100 nM), indicating that it arose from augmentation of KCNQ subfamily and KCNA3 but not KCNA1 K^+ channel activity. *Kcne2* deletion in C57B6 mice also altered the polarity of CPe KCNQ1 and KCNA3 trafficking, hyperpolarized the CPe membrane by 9 ± 2 mV, and increased CSF [Cl^-] by 14% compared with wild-type mice. These findings constitute the first report of CPe dysfunction caused by cation channel gene disruption and suggest that KCNE2 influences blood-CSF anion flux by regulating KCNQ1 and KCNA3 in the CPe.—Roepke, T. K., Kanda, V. A., Purtell, K., King, E. C., Lerner, D. J., Abbott, G. W. KCNE2 forms potassium channels with KCNA3 and KCNQ1 in the choroid plexus epithelium. *FASEB J.* 25, 4264–4273 (2011). www.fasebj.org**

Key Words: MiRP1 · cerebrospinal fluid · polarized trafficking · central nervous system · ventricles

Cerebrospinal fluid (CSF), secreted by the ependymal cells of the choroid plexus (CP), has numerous important functions, including physical support for and protection of the CNS, delivery of nutrients to and removal of waste products from the CNS, and physical communication between different CNS structures. Abnormal CSF production and/or absorption can cause common clinical problems, including cerebral edema and intracranial hypertension; drugs that reduce CSF production are effective for treating these conditions (1). Identification of novel drug targets in the choroid plexus epithelium (CPe) to manipulate specific CPe transport processes could open therapeutic avenues for a diverse range of disorders (2).

Voltage-gated potassium (Kv) channel α subunits KCNA1, KCNA3, and KCNA6 (also named Kv1.1, Kv1.3, and Kv1.6, respectively) and inward rectifier K^+ channel α subunit KCNJ13 (Kir7.1) have all been detected at the CPe apical membrane. They are thought to contribute to apical K^+ efflux (3–5), potentially providing a leak pathway for K^+ ions pumped into the cell by the Na^+,K^+-ATPase and to maintenance of the negative cell membrane potential (E_m), which is important in establishing the electrochemical gradient for anion efflux needed to drive CSF secretion (3). CPe K^+ transport from the CSF to the blood is vital in maintaining CSF [K^+] close to 3 mM, even when plasma [K^+] is experimentally varied over a range of 2 to 11 mM (6) and is thus essential for the normal activity of the CNS.

Kv α subunits form complexes with a range of ancillary subunits, such as the single-transmembrane domain proteins encoded by the *KCNE* gene family (ref. 7 and **Fig. 1*A***). We previously found that variants in the gene encoding KCNE2 (a protein we originally termed MinK-related peptide 1) associate with inherited and drug-induced forms of the cardiac arrhythmia, long QT syndrome (LQTS; refs. 8, 9). More recently, *KCNE2* sequence variants or gene duplications have been tentatively associated with a human cardiocerebral phenotype comprising both neonatal seizures and LQTS (10) and with schizophrenia (11), suggesting potential cerebral functions for KCNE2, but *KCNE2* transcript levels in human neuronal tissue appear relatively low (12). However, *KCNE2* transcripts are reportedly highly enriched in the fourth and lateral ventricles

[1] Current address: Clinic for Cardiology and Angiology, Charite University-Medicine Berlin, Campus Mitte and Experimental and Clinical Research Center, Max Delbrueck Center for Molecular Medicine, Berlin, Germany.

[2] Current address: Tyrx Inc., Monmouth Junction, NJ, USA.

[3] Correspondence: Department of Pharmacology, Box 70, Weill Cornell Medical College, 1300 York Ave., New York, NY 10021, USA. E-mail: gwa2001@med.cornell.edu

doi: 10.1096/fj.11-187609

0892-6638/11/0025-4264 © FASEB

(ref. 13; see http://mouse.brain-map.org) and have been detected in the CPe (14).

Here, we found that KCNE2 protein is prominently expressed in the apical membrane of the CPe, where we also discovered the KCNQ1 (Kv7.1) Kv channel α subunit. We report that KCNE2 forms K^+ channels with KCNQ1 and KCNA3 α subunits in the CPe apical membrane and that targeted *Kcne2* deletion in mice alters CPe outward K^+ current, membrane potential and K^+ channel trafficking, and CSF [Cl^-].

MATERIALS AND METHODS

Animal use

We generated and genotyped the *Kcne2*$^{-/-}$ mouse line as described previously (15, 16) and housed and used mice according to the National Institutes of Health Guide for the Care and Use of Laboratory Animals. Animal procedures were approved by the institutional animal care and use committee at Weill Medical College of Cornell University.

Data presentation, statistics, and nomenclature

Data are expressed as means ± SE of n independent measurements. Statistical comparisons were generally by 1- or 2-tailed unpaired Student's t test or 1-way ANOVA followed by the Bonferroni *post hoc* test. In all cases, statistical significance was assumed with $P < 0.05$. For genes and proteins, the International Union of Basic and Clinical Pharmacology-recommended nomenclature is followed, but other names are also given; thus, MinK-related proteins are referred to by their KCNE designation and K^+ channel α subunits by their KCN(X) designation. In addition, as per convention, human protein names are in uppercase, human genes are in uppercase italics, mouse proteins are in lowercase (but beginning with an uppercase letter), and mouse genes are in lowercase italics (but beginning with an uppercase letter).

Immunohistochemistry and immunofluorescence

Tissue samples from *Kcne2*$^{+/+}$ and *Kcne2*$^{-/-}$ mice were fixed in 4% paraformaldehyde solution (Electron Microscopy Sciences, Hatfield, PA, USA), followed by incubation in 30% sucrose overnight at 4°C. Embedding was performed in OCT compound (Tissue-Tek, Torrance, CA, USA), and embedded samples were stored at −80°C. Frozen samples were cut into 10-μm-thick sections (Cryomicrotome CM 1850; Leica Microsystems, Bannockburn, IL, USA). Immunohistochemical detection of Kcnq1 and Kcne2 was performed with a Discovery XT System (Ventana Medical Systems, Tucson, AZ, USA). For single labeling with diaminobenzidine detection, a 30-min blocking step was used, with 10% normal goat serum (when rabbit polyclonal antibodies were used) or rabbit serum (when goat polyclonal antibodies were used) and 2% BSA followed by avidin and biotin incubation for 4–8 min each. Primary antibody incubation was performed at room temperature using goat polyclonal anti-KCNQ1 (pan-species) primary antibody (SC-10646; Santa Cruz Biotechnology, Inc., Santa Cruz, CA, USA) at 1 mg/ml; in-house rabbit polyclonal, site-directed anti-KCNE2 (pan-species) serum was diluted 1:5000 after column-enriching IgG. This was followed by 60 min of incubation with biotinylated secondary antibodies at 1:200 dilution (Vector Laboratories, Burlingame, CA, USA). A diaminobenzidine detection kit containing Blocker D, Copper D, Inhibitor D, streptavidin horseradish peroxidase D, and diaminobenzidine D (Ventana Medical Systems) was used according to the manufacturer's instructions. Slides were viewed with a Nikon Eclipse E600 microscope (Nikon, Tokyo, Japan) and photographed using an RT Color Camera and SPOT software (Diagnostic Instruments, Inc., Sterling Heights, MI, USA).

Immunofluorescence detection of Kcne2, Kcnq1, Kcna3, and Nkcc1 was performed using a Discovery XT processor (Ventana Medical Systems). Goat polyclonal anti-KCNQ1 (pan-species) primary antibody (SC-10646; Santa Cruz Biotechnology, Inc.) was used at 1 mg/ml, in-house rabbit polyclonal, site-directed anti-KCNE2 (pan-species) serum was diluted 1:5000 after column-enriching IgG, mouse monoclonal anti-KCNA3 (75-009; NeuroMab, University of California, Davis, CA, USA) was diluted 1:500, and rabbit or goat polyclonal anti-NKCC1 (Santa Cruz Biotechnology, Inc.) was diluted 1:1000. Preceding the primary antibody incubation, tissue sections were blocked for 30 min in 10% normal goat serum (for slides stained with a combination of mouse and rabbit primary and secondary antibodies), rabbit serum (for slides stained with a combination of mouse and goat primary and secondary antibodies), or mouse serum (for slides stained with a combination of rabbit and goat primary and secondary antibodies) and 2% BSA in PBS, followed by an 8-min avidin/biotin block. The primary antibody incubation (3 h) was followed by incubation with biotinylated anti-rabbit, anti-mouse, or anti-goat IgG as appropriate (ABC kit; Vector Laboratories). The secondary detection was performed with streptavidin-horseradish peroxidase D (Ventana Medical Systems), followed by incubation with tyramide Alexa Fluor 488 (Invitrogen, Carlsbad, CA, USA) or tyramide Alexa Fluor 568 (Invitrogen). Immunostained slides were viewed with a Zeiss Axiovert 200 widefield microscope, and pictures were acquired using MetaMorph 7.1 software (Molecular Devices, Sunnyvale, CA, USA).

Choroid plexus harvesting and preparation for cellular electrophysiology or biochemistry

Adult *Kcne2*$^{+/+}$ and *Kcne2*$^{-/-}$ mice were killed by CO_2 asphyxiation, and the choroid plexus was removed from the fourth ventricle of the brain. Tissue samples were then kept in ice-cold, control bath solution (140 mM NaCl, 5 mM KCl, 1 mM $CaCl_2$, 1 mM $MgCl_2$, 5 mM HEPES, 10 mM mannitol, and 5 mM glucose, adjusted to pH 7.3 with NaOH; osmolality=298±4 mosmol/kg H_2O, n=6) and used in patch-clamp experiments within 3 h of isolation; or snap-frozen in liquid N_2 for use in Western blot analysis.

CSF extraction and ion quantification

CSF was isolated from the cisterna magna of 3- to 6-mo-old *Kcne2*$^{+/+}$ and *Kcne2*$^{-/-}$ mice using a modification of a technique described previously (17). In brief, mice were initially anesthetized with 1% isoflurane in 100% oxygen in a Plexiglas chamber and then placed in a small animal stereotactic apparatus (model 900; David Kopf Instruments, Tujunga, CA, USA) fitted with a mouse anesthesia mask (David Kopf Instruments) and ear bars to minimize movement of the head. With the head locked in place, the body of the mouse was allowed to drop to give access to the neck region. The neck was shaved, an incision was made using a sterile scalpel (no. 10 blade), and the muscles

of the neck were separated by blunt dissection to reveal the cisterna magna. Glass borosilicate capillary tubes (B100–78-10; Sutter Instrument, Novato, CA, USA), pulled on a vertical micropipette puller (PP-830; Narishige, Tokyo, Japan) to generate a tapered tip with an inner diameter of roughly 0.6 mm, were then used to penetrate the cisterna magna, and CSF was drawn into the capillary tubes. A 1-ml syringe with polyethylene tubing attached to the end (to allow tight connection with the capillary tube) was then used to remove the CSF from the capillary tube. CSF samples were placed on dry ice and stored at −80°C until analysis. Mice were then killed by CO_2 asphyxiation.

CSF [K^+] was analyzed by AniLytics (Gaithersburg, MD, USA) using a K^+ ion-selective electrode. CSF pH measurements were conducted using a pH glass microelectrode (Microelectrodes, Inc., Bedford, NH, USA). CSF [Cl^-] was determined using a QuantiChrom colorimetric chloride assay kit (Bioassay Systems, Hayward, CA, USA) following the manufacturer's protocol. In brief, nonpooled 1-μl CSF samples from 6-mo-old *Kcne2*$^{+/+}$ and *Kcne2*$^{-/-}$ mice were diluted 20-fold, as per the manufacturer's protocol for biological samples, and 5 μl of each dilution was independently tested 6 times for [Cl^-]. The absorbance of each data point was read at 610 nm using a VERSAmax tunable microplate reader (Molecular Devices) and analyzed using SoftMax Pro 4.8 (Molecular Devices). The absorbance readings were converted to [Cl^-] (mM) by direct comparison to a [Cl^-] standard curve.

Western blot analysis

Cell lysates from choroid plexus epithelia of the fourth ventricle were pooled from either 20 *Kcne2*$^{+/+}$ or *Kcne2*$^{-/-}$ mice and isolated according to Speake *et al.* (18) with centrifugation to remove nuclear material, or whole CPe lysates from individual mice without removal of nuclear material were used. This difference in preparation had no noticeable effect on membrane protein subunit band patterns, but if nuclear material was not removed, an additional glyceraldehyde 3-phosphate dehydrogenase (GAPDH) band was observed. The lysates were resolved using SDS-PAGE and transferred to PVDF membranes for Western blot analysis using standard techniques and equipment (Bio-Rad Laboratories, Hercules, CA, USA). PVDF membranes were incubated for 3 h at room temperature in 5% milk with primary antibodies, diluted as follows: rabbit polyclonal Kcne2 (in-house) 1:1000; goat polyclonal Kcnq1 (Santa Cruz Biotechnology, Inc.) 1:1000; mouse monoclonal Kcna3 (NeuroMab) 1:500; mouse monoclonal Kcna1 (Chemicon International, Temecula, CA) 1:1000; mouse monoclonal Kcna6 (Chemicon International) 1:500; goat polyclonal Kcnj13 (Santa Cruz Biotechnology, Inc.) 1:500; NKCC1 (Santa Cruz Biotechnology, Inc.) 1:500; AQP1 (Chemicon International) 1:1000; and GAPDH (Bio-Rad Laboratories) 1:100. For secondary detection, horseradish peroxidase-conjugated species-appropriate anti-IgG antibodies (1:10.000, Bio-Rad Laboratories) were used. Signals were detected with ECL-Plus chemiluminescence (Amersham Biosciences, Piscataway, NJ, USA), were visualized by fluorography, and, where indicated, were quantified using densitometry as we reported previously (16).

Electrophysiology

K^+ channel activity in CPe cells isolated from 3-mo-old *Kcne2*$^{+/+}$ and *Kcne2*$^{-/-}$ mice was recorded by whole-cell patch-clamp methods. Briefly, small pieces of choroid plexus tissue, bathed in the control bath solution, were affixed to Cell-Tak-coated coverslips and transferred to a perfusion chamber (bath volume 400 μl) mounted on the stage of an inverted microscope (Olympus, Tokyo, Japan). Patch pipettes were made from hematocrit capillary tubes (Oxford Labware, Mansfield, MA, USA) with a vertical micropipette puller. The tip resistances of the patch pipettes were 3–5 MΩ. Conventional whole-cell patch-clamp recordings were performed at 22–25°C after gigaohm seals had been obtained on the exposed apical membrane of the epithelial cells. Whole-cell currents (voltage-clamp mode)

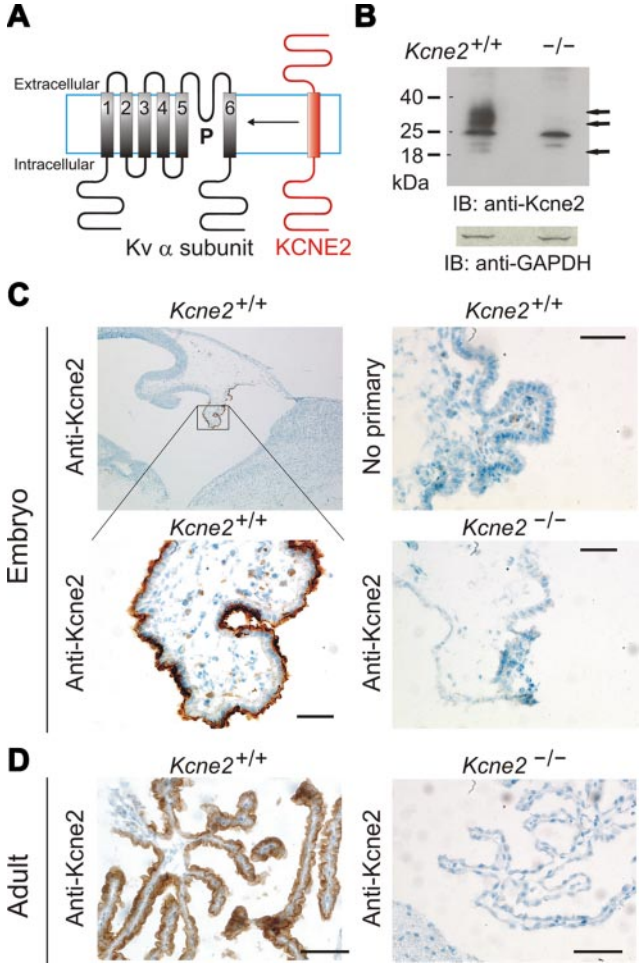

Figure 1. Kcne2 is expressed apically in the CPe. *A*) Schematic representation of a Kv α subunit and KCNE2 showing transmembrane topology. P is the pore loop; Kv α subunit transmembrane segments are labeled 1–6. *B*) Top: Western blot of mouse CPe cell lysates, using anti-Kcne2 antibody. Arrows, bands in *Kcne2*$^{+/+}$ CPe lane that are absent from the *Kcne2*$^{-/-}$ CPe lane, with electrophoretic migration consistent with 0-, 1-, and 2-glycosylated forms of Kcne2. Bottom: Western blot with anti-GAPDH antibody indicating equal total protein concentrations for *Kcne2*$^{+/+}$ and *Kcne2*$^{-/-}$ CPe lysates. Representative of $n = 2$ experiments, each using pooled choroid plexus lysates from 20 mice/genotype. IB, immunoblot. *C*) Immunohistochemical analysis of embryonic *Kcne2*$^{+/+}$ and *Kcne2*$^{-/-}$ mouse CPe, showing immunoreactivity with anti-Kcne2 antibody in *Kcne2*$^{+/+}$ but not *Kcne2*$^{-/-}$ CPe and no immunoreactivity without the primary antibody. Representative of $n = 4$ tissue sections. *D*) Immunohistochemical analysis of adult *Kcne2*$^{+/+}$ and *Kcne2*$^{-/-}$ mouse CPe, showing immunoreactivity with anti-Kcne2 antibody in *Kcne2*$^{+/+}$ but not *Kcne2*$^{-/-}$ CPe. Representative of $n = 3$ tissue sections. Scale bars = 20 μm (*C*);100 μm (*D*).

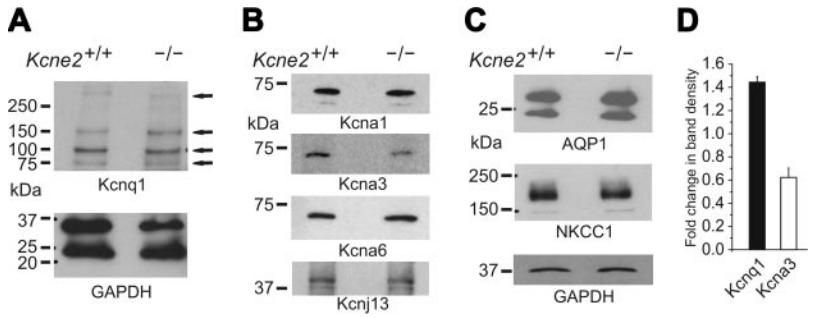

Figure 2. Expression of K^+ channels, AQP1 and NKCC1, in the CPe of *Kcne2*$^{+/+}$ and *Kcne2*$^{-/-}$ mice. *A*) Western blot of mouse CPe cell lysates, using anti-Kcnq1 antibody (top) and corresponding blot for anti-GAPDH antibody as a loading control (bottom). Arrows represent bands corresponding to expected weights for various multimeric forms of Kcnq1. Representative of $n = 3$ experiments, each using either pooled choroid plexus lysates with the nuclear fraction removed by centrifugation from 20 mice/genotype or whole choroid plexus lysate from individual mice (as in the blot shown here; hence, 2 bands are observed for GAPDH, corresponding to nuclear and cytosolic forms of GAPDH). *B*, *C*) Western blots of mouse *Kcne2*$^{+/+}$ and *Kcne2*$^{-/-}$ CPe cell lysates, using commercial antibodies raised against the various ion channel α subunits (*B*) and transporters (*C*) shown and GAPDH as a loading control. Representative of $n = 3$ experiments, each using pooled choroid plexus lysates with nuclear fraction removed by centrifugation from 20 mice/genotype (as in the blot shown here; hence, a single band for GAPDH corresponding to the cytosolic form only) or whole choroid plexus lysate from individual mice. *D*) Mean fold change in band density for Kcnq1 (n=3) and Kcna3 protein (n=4) in *Kcne2*$^{-/-}$ *vs.* *Kcne2*$^{+/+}$ CPe cell lysates (*i.e.*, effect of *Kcne2* deletion). Error bars = SE.

were measured with a Multiclamp 700A Amplifier, a Digidata 1300 Analog/Digital converter, and pClamp9 software (Axon Instruments, Foster City, CA, USA). Leak and liquid junction potentials (<4 mV) were not compensated for when current-voltage relationships were generated. Kv channel-specific blockers (XE991, 10 μM; margatoxin, 10 μM; and dendrotoxin, 100 nM) were applied directly to the bath. Current-voltage (*I/V*) relationships are for the maximum current measured at each V_m. Current decay was fit with a single exponential to determine the inactivation rate. Data analysis was performed using Clampfit 9 (Axon Instruments) and Origin 6.1 (MicroCal; GE Healthcare, Piscataway, NJ, USA). Currents were normalized for whole-cell capacitance and are expressed as amperes per farad.

For patch-clamp recording from cloned channels in CHO cells, 5×10^5 cells were plated in 60-mm tissue culture dishes 1 day before transfection. CHO cells were transiently transfected using SuperFect transfection reagent (Qiagen, Hilden, Germany) following the manufacturer's protocol. Cells were transfected with cDNA as follows: 0.1 μg (unless otherwise noted) of murine Kcna1 or Kcna3 alone or in combination with 0.5 μg of murine Kcne2 cDNA and an empty vector (pBluescript) to enhance transfection efficiency. Cells were cotransfected with a plasmid cDNA encoding enhanced green fluorescent protein (pBOB-EGFP) to visualize transfected cells for whole-cell voltage-clamp experiments. Experiments were performed 24 h post-transfection. Cells were perfused with an extracellular bath solution containing 135 mM NaCl, 5 mM KCl, 1.2 mM $MgCl_2$, 5 mM HEPES, 2.5 mM $CaCl_2$, and 10 mM D-glucose (pH 7.4). Patch electrodes were pulled from standard-walled, borosilicate glass capillaries with filament (Sutter Instrument) using a P-97 horizontal puller (Sutter Instrument) and had resistances of 3–5 MΩ when filled with intracellular solution containing 10 mM NaCl, 117 mM KCl, 2 mM $MgCl_2$, 11 mM HEPES, 11 mM EGTA, and 1 mM $CaCl_2$ (pH 7.2). Data were filtered at 1 kHz and digitized at 5 kHz using a Digidata 1322A analog-to-digital converter (Axon Instruments). Leak and liquid potentials were not compensated for.

RESULTS

Kcne2 and Kcnq1 are expressed in the CPe

Western blotting of mouse CPe lysates, with *Kcne2*$^{-/-}$ mouse CPe lysates as a negative control, indicated Kcne2 expression in the *Kcne2*$^{+/+}$ mouse CPe (Fig. 1*B*). Furthermore, using immunohistochemical analysis and with *Kcne2*$^{-/-}$ mouse CPe lysates or omission of primary antibody as negative controls, we found cerebral Kcne2 protein expression to be strikingly enriched in the apical membrane of the CPe of both embryonic (Fig. 1*C*) and adult (Fig. 1*D*) mice.

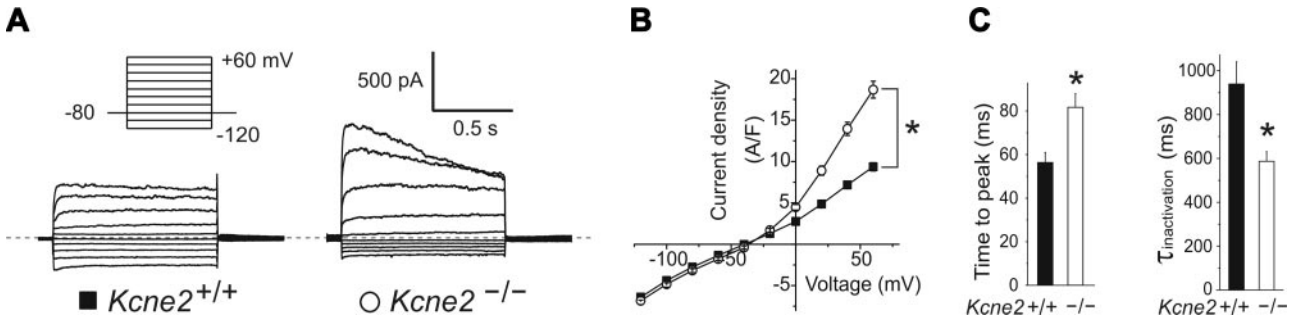

Figure 3. *Kcne2* deletion increases outward K^+ current in the CPe. *A*) Exemplar whole-cell current recordings from isolated CPe cells using 5 mM K^+ bath solution and the voltage protocol indicated. *B*) Mean current density-voltage relationship for cells as in *A*; $n = 28$–39 cells/genotype; $^*P < 0.001$ for outward currents. *C*) Left panel: mean time-to-peak current at +60 mV for cells as in *B*; $n = 28$–39 cells/genotype; $^*P < 0.001$. Right panel: mean inactivation τ at +60 mV for cells as in *B*; $n = 28$–39 cells/genotype; $^*P < 0.001$.

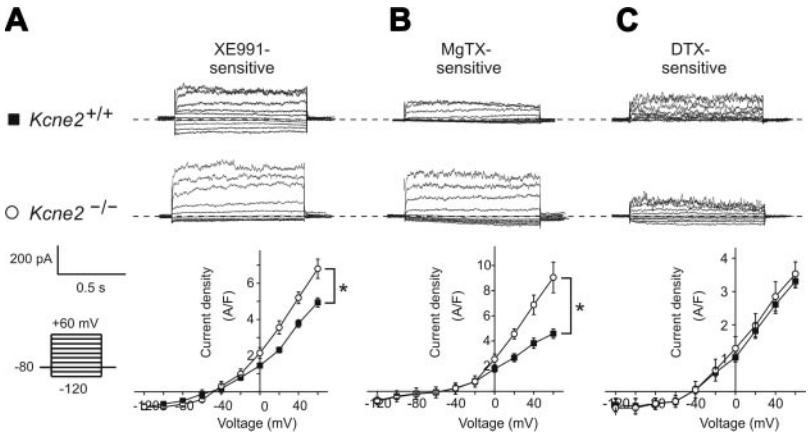

Figure 4. Kcne2 regulates Kcnq1 and Kcna3, but not Kcna1, in the CPe. *A–C*) Top panels: exemplar whole-cell native CPe currents sensitive to the agents indicated [*A*) 10 μM XE991; *B*) 10 μM margatoxin (MgTX); *C*) 100 nM dendrotoxin (DTX)], computed using digital subtraction of postdrug currents from predrug currents and the voltage protocol indicated. Dashed line indicates 0 current level. Bottom panels: mean current density-voltage relationship for drug-sensitive currents as above; $n = 7$ cells/genotype for *Kcne2*$^{-/-}$ and *Kcne2*$^{+/+}$ (XE991); $n = 4$ cells/genotype for *Kcne2*$^{-/-}$ and $n = 7$ cells/genotype for *Kcne2*$^{+/+}$ (MgTX); and $n = 5$ cells/genotype for *Kcne2*$^{-/-}$ and $n = 6$ cells/genotype for *Kcne2*$^{+/+}$ (DTX). $^*P < 0.05$.

We also discovered that Kcnq1, a K^+ channel α subunit partner of Kcne2 in the stomach and thyroid (15, 19), is expressed in the CPe. Using Western blotting of lysates pooled from the CPe of 20 mice and GAPDH expression as a loading control, we discovered that *Kcne2* deletion resulted in up-regulation of CPe Kcnq1 expression (**Fig. 2*A*, *D***), as we previously observed in the stomach mucosa of *Kcne2*$^{-/-}$ mice (15). Analyzing the other known CPe K^+ channels, again using Western blotting of CPe lysates pooled from 20 mice/genotype, we found that *Kcne2* deletion appeared to decrease CPe Kcna3 protein expression but had no effect on the expression of the other known CPe K^+ channel proteins, Kcna1 (Kv1.1), Kcna6 (Kv1.6), or Kcnj13 (Kir7.1) (Fig. 2*B, D*). Similarly, *Kcne2* deletion did not alter levels of two other known CPe membrane proteins, aquaporin 1 (AQP1) and NKCC1 (Fig. 2*C*).

Kcne2 deletion increases CPe cell Kcna3 and Kcnq1 outward current density

Patch-clamp recordings in whole-cell configuration from isolated *Kcne2*$^{+/+}$ mouse CPe cells bathed in 5 mM K^+ solution exhibited an almost linear current-voltage relationship, whereas *Kcne2*$^{-/-}$ CPe cell K^+ current exhibited increased outward rectification, with a 2-fold increased mean outward current density compared with *Kcne2*$^{+/+}$ CPe cells (**Fig. 3*A*, *B***). The outward current in *Kcne2*$^{-/-}$ CPe cells also exhibited slower voltage-dependent activation and faster inactivation than that of *Kcne2*$^{+/+}$ CPe cells (Fig. 3*C*).

We next used Kv channel antagonists to determine the molecular correlates of the outward current altered by *Kcne2* deletion, focusing on Kcna1, Kcna3, and Kcnq1. The mean density of the CPe outward current component sensitive to the Kcnq-specific antagonist XE991 was increased 25% by *Kcne2* deletion, and the outward rectification of the XE991-sensitive current was also increased (**Fig. 4*A***). CPe outward current sensitive to the Kcna3-specific antagonist margatoxin was increased 2-fold by *Kcne2* deletion, with the small amount of inward current remaining unchanged (Fig. 4*B*). In contrast, CPe Kcna1 current, identified by dendrotoxin sensitivity, was unchanged by *Kcne2* deletion (Fig. 4*C*).

These changes in XE991-sensitive current (Fig. 4*A*) are consistent with loss of Kcne2 from Kcnq1-Kcne2 complexes, because Kcne2 reduces the voltage dependence of Kcnq1 activation (and thus reduces outward rectification) and decreases its macroscopic outward current amplitude (20). The changes could also reflect the increase in Kcnq1 protein membrane expression suggested by data herein (Fig. 2*A*).

The increased Kcna3 current appeared paradoxical because total Kcna3 protein expression in the CPe was reduced by *Kcne2* deletion (Fig. 2*B*). Furthermore, Kcne2 has not previously been reported to

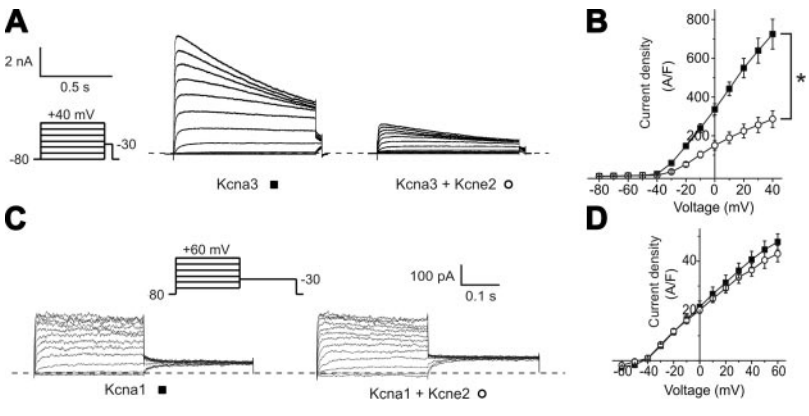

Figure 5. Kcne2 partially suppresses Kcna3 but not Kcna1 current *in vitro*. *A*) Exemplar whole-cell currents in CHO cells transfected with rat Kcna3 cDNA alone or with mouse Kcne2 cDNA, using 5 mM K^+ bath solution and the protocol indicated. Dashed line indicates 0 current level. *B*) Mean current density-voltage relationship for cells as in *A*; $n = 8$–9 cells/group. $^*P < 0.001$ for outward currents. *C*) Exemplar whole-cell currents in CHO cells transfected with rat Kcna1 cDNA alone or with mouse Kcne2 cDNA, using 5 mM K^+ bath solution and the protocol indicated. Dashed line indicates 0 current level. *D*) Mean current density-voltage relationship for cells as in *C*; $n = 15$–18 cells/group. $P > 0.05$ (no significant difference between groups).

modulate Kcna3, and human KCNE2 was previously found to have no effect on rat Kcna3 function when coexpressed in human embryonic kidney (HEK) cells (21). To understand this apparent paradox, we determined the functional effects of murine Kcne2 and Kcna3 heterologous coexpression in CHO cells and found that Kcne2 inhibited Kcna3 current by 60% (**Fig. 5*A*, *B***) but did not alter the function of Kcna1 in similar experiments (Fig. 5*C*, *D*). This result provided a qualitative explanation for our findings with native CPe Kcna3 current (Fig. 4*B*) and also for the lack of effects of *Kcne2* deletion on native CPe Kcna1 current (Fig. 4*C*) and constitutes the first report of Kcna3 modulation by Kcne2 (*in vivo* or *in vitro*).

Summation of the CPe current densities for each of the three current components studied (XE991-, margatoxin-, and dendrotoxin-sensitive) was sufficient to account for all of the outward current for each genotype and thus also for the current density changes caused by *Kcne2* deletion (Figs. 2 and 3). Thus, *Kcne2* deletion increased CPe Kcnq1 and Kcna3 outward current density and outward rectification, with no effect on Kcna1. Furthermore, the functional changes were consistent with direct functional regulation of Kcnq1 and Kcna3 by Kcne2 in wild-type mouse CPe.

Kcne2 deletion alters the trafficking polarity of Kcna3 and Kcnq1 in the CPe

Given the functional data suggesting regulation of Kcnq1 and Kcna3 by Kcne2 in the CPe, we examined localization of these subunits in the CPe using immunofluorescence. First, we again detected Kcne2 in the apical membrane of the CPe, using single labeling with anti-Kcne2 antibody, DAPI staining of nuclei, and the CPe of $Kcne2^{-/-}$ mice as a negative control (**Fig. 6*A***). Next, using single labeling with anti-Kcnq1 antibody and DAPI staining of nuclei, we found that Kcnq1 appeared to localize to the apical membrane of the CPe in $Kcne2^{+/+}$ mice but to the basolateral membrane and/or intracellular compartment of the CPe in $Kcne2^{-/-}$ mice (Fig. 6*B*).

Using double labeling with rabbit anti-Kcne2 antibody and goat anti-Kcnq1 antibody, we found that Kcne2 and Kcnq1 partially colocalize in the CPe apical membrane. Fainter Kcnq1 staining was also observed in other areas, but where it was strongest at the CPe apical membrane, Kcne2 was strongly colocalized with it (Fig. 6*C*). The NKCC1 transporter is an established marker of the CPe apical membrane (22); therefore, we next used double-labeling with rabbit anti-NKCC1 antibody and goat anti-Kcnq1 antibody to verify the aberrant Kcnq1 trafficking observed with single labeling in the CPe of $Kcne2^{-/-}$ mice (Fig. 6*B*). In $Kcne2^{+/+}$ CPe, strongly overlapping KCNQ1 and NKCC1 signals were observed, confined specifically to the CPe (Fig. 6*D*, *E*). In contrast, in $Kcne2^{-/-}$ mice, although anti-NKCC1 antibody staining was consistent with an apical location as previously reported (22), Kcnq1 staining did not colocalize with NKCC1, but was in the basolateral and/or intracellular compartments (Fig. 6*F*). Thus, both single- and double-labeling experiments suggested that Kcnq1 colocalized apically with Kcne2 in the CPe of wild-type mice, but that in the CPe of $Kcne2^{-/-}$ mice, Kcnq1 did not reach the apical membrane.

Kcna3 was previously identified in the CPe apical membrane (4). Here, using double labeling with mouse anti-Kcna3 and rabbit anti-Kcne2 antibodies, we found that Kcna3 colocalized with Kcne2 in the $Kcne2^{+/+}$ CPe, as expected, because both are apical (Fig. 6*G*). We could not obtain sufficient resolution with this combination of antibodies in wild-type CPe to interpret further than this, although in further support of an apical localization for Kcna3 in $Kcne2^{+/+}$ CPe, we also observed at least partial colocalization of Kcna3 and NKCC1 in $Kcne2^{+/+}$ CPe (Fig. 6*H*). In contrast, when double-labeling CPe from $Kcne2^{-/-}$ mice with rabbit anti-NKCC1 and mouse anti-Kcna3 antibodies, we saw no colocalization: NKCC1 was apically located, but Kcna3 was very distinctly localized to the basolateral compartment (Fig. 6*I*).

Kcne2 deletion hyperpolarizes CPe E_m and reduces CSF but not serum [Cl^-]

Given that Kcne2 altered CPe K^+ currents, which are frequently influential in setting resting E_m, we next measured resting E_m in CPe cells isolated from $Kcne2^{+/+}$ and $Kcne2^{-/-}$ mice. These experiments revealed a statistically significant 9 ± 2 mV hyperpolarizing shift due to *Kcne2* deletion (**Table 1**). This result is consistent with the increased K^+ efflux we observed in CPe cells isolated from $Kcne2^{-/-}$ mice (Figs. 3 and 4), as K^+ conductance drives the cell membrane potential toward the K^+ equilibrium potential, E_K. This hyperpolarization would be expected to increase anion efflux from the CPe into the CSF. We found mildly (14%) increased CSF [Cl^-] in $Kcne2^{-/-}$ mice compared with that in $Kcne2^{+/+}$ mice (134±6 *vs.* 118±5 mM, respectively, measurements performed on 6 aliquots each from independent CSF samples of n=5 mice/genotype, $P<0.05$, 1-tailed Student's t test). In contrast, there were no changes in serum [Cl^-], CSF pH, or CSF [K^+] apparent with *Kcne2* deletion (Table 1).

DISCUSSION

KCNE2 and KCNQ1 were each originally described as subunits contributing to the two major human cardiac ventricular repolarization currents: KCNE2 in complexes with human *ether-a-go-go*-related gene generating I_{Kr} and KCNQ1 in complexes with KCNE1 generating I_{Ks} (7). KCNQ1 and KCNE2 were later discovered to form a constitutively active channel together *in vitro* (20), and found to provide a parietal cell apical K^+ efflux pathway essential for gastric acid

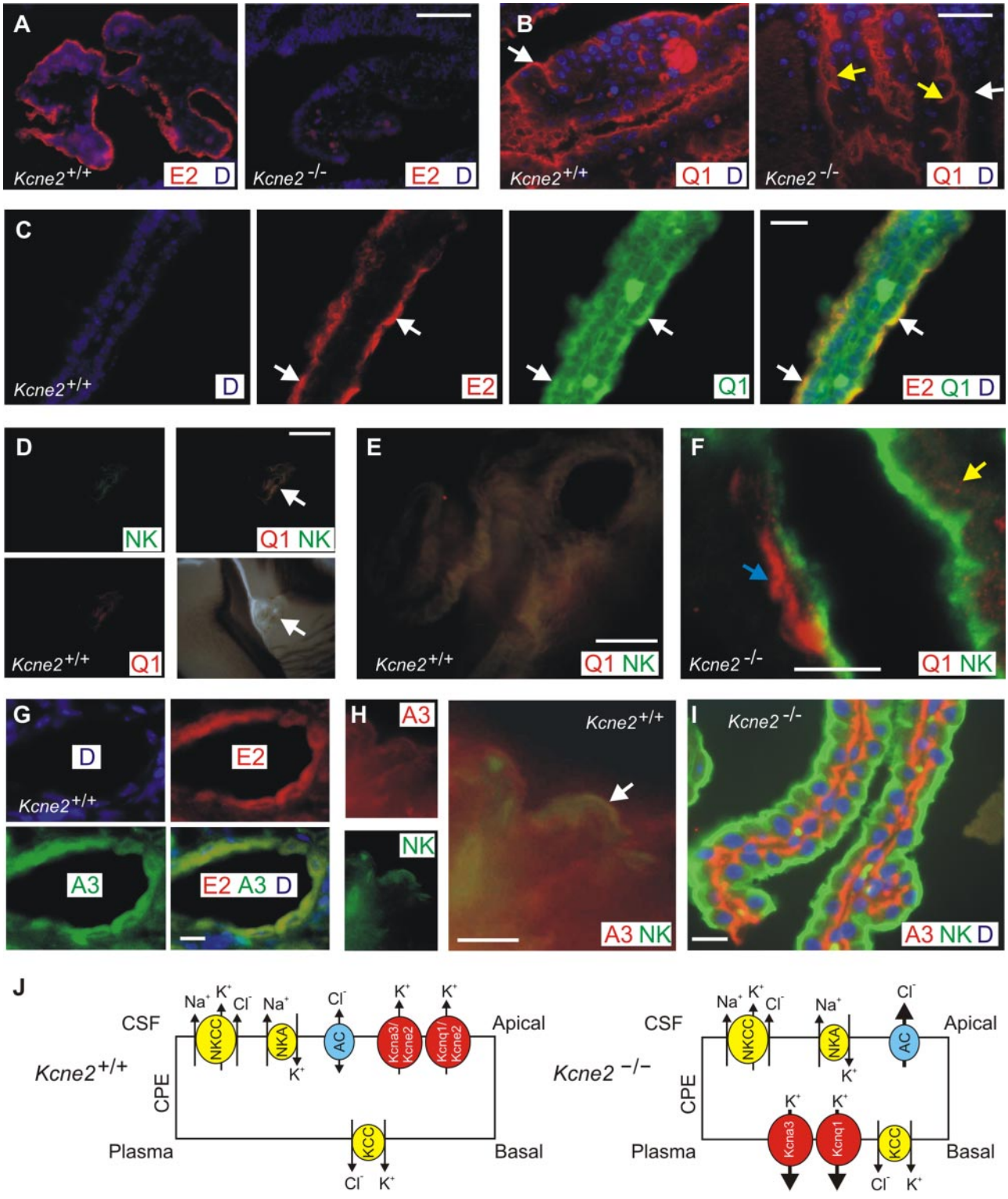

Figure 6. Kcna3 and Kcnq1 localization in *Kcne2*$^{+/+}$ and *Kcne2*$^{-/-}$ mouse CPe. *A*) Immunofluorescence of embryonic *Kcne2*$^{+/+}$ and *Kcne2*$^{-/-}$ mouse CPe, showing immunoreactivity with anti-Kcne2 antibody (E2, red) in *Kcne2*$^{+/+}$ but not *Kcne2*$^{-/-}$ CPe; DAPI staining (D, blue). Representative of $n = 3$ tissue sections. *B*) Immunofluorescence of adult *Kcne2*$^{+/+}$ and *Kcne2*$^{-/-}$ mouse CPe, showing immunoreactivity with anti-Kcnq1 antibody (Q1, red) in the apical membrane of *Kcne2*$^{+/+}$ mouse CPe but in the basolateral and/or intracellular compartment of *Kcne2*$^{-/-}$ mouse CPe; DAPI staining (D, blue). Representative of $n = 3$ tissue sections. White arrows, apical membrane; yellow arrows, basal membrane. *C*) Immunofluorescence of adult *Kcne2*$^{+/+}$ mouse CPe, showing apical localization of Kcne2 (E2, red) and Kcnq1 (Q1; green); white arrows indicate colocalization; DAPI staining (D, blue). Representative of $n = 3$ tissue sections. *D*) Immunofluorescence of adult *Kcne2*$^{+/+}$ mouse CPe, showing signal for Kcnq1 (Q1, red) and NKCC1 (NK, green) only in the CPe, with no staining in neighboring neuronal tissue (bottom right, bright field image of the same region for comparison). White arrowhead, CPe. Representative of $n = 2$ tissue sections.

(*continued on next page*)

TABLE 1. *Effects of* Kcne2 *deletion on CPe and CSF parameters*

Genotype	CPe E_m (mV)	CSF pH	CSF $[K^+]$ (mM)	Serum $[Cl^-]$ (mM)	CSF $[Cl^-]$ (mM)
Kcne2$^{+/+}$	−39.5 ± 1.5 (10)	7.5 ± 0.3 (10)	3.2 (9)	107 ± 1 (6)	118 ± 5 (5)
Kcne2$^{-/-}$	−48.1 ± 1.9 (12)*	7.3 ± 0.4 (10)	3.1 (10)	111 ± 1 (6)	134 ± 6 (5)*

CPe and CSF parameters are indicated as means ± SE, where available, with n values in parentheses; absence of SE indicates that intragenotype samples were pooled before measurement. *$P < 0.05$ *vs.* *Kcne2*$^{+/+}$.

secretion (15, 23). The KCNQ1-KCNE2 channel is also expressed at the basolateral membrane of thyrocytes (19).

Unlike KCNQ1, KCNA3 retains its voltage dependence when coexpressed with KCNE2, but its currents are partially suppressed. As with some other KCNE2-α subunit partnerships, there is cell type- and/or KCNE species-specific dependence to this interaction: in another recent study, human KCNE2 was found not to modulate rat Kcna3 function in HEK cells (21). Consistent with this finding, we previously found that rat KCNE2 functionally regulates KCNC1 (Kv3.1) and KCNC2 (Kv3.2) in CHO cells, whereas human KCNE2 does not (24). The mechanistic basis for this difference is not yet known; one or more of the 24 nonconserved amino acid residues between rat and human KCNE2 (8) may underlie the disparity, or it could relate to cell-type specific regulatory processes we do not yet understand. The finding here that *Kcne2* deletion shifts KCNA3 and KCNQ1 trafficking to the CPe basolateral membrane recapitulates our recent finding of the same reversal in trafficking polarity of KCNQ1 in gastric parietal cells (25). The α subunit rerouting may be a determining factor in the CPe dysfunction in *Kcne2*$^{-/-}$ mice, although the simple increase in KCNA3 and KCNQ1 outward currents could also explain the observed effects.

KCNQ1-KCNE2 and KCNA3-KCNE2 channels probably do not play a major part in regulating baseline CSF $[K^+]$. *Kcne2* disruption here did not result in altered baseline CSF $[K^+]$, and the most important regulator of CSF $[K^+]$ is probably active K^+ removal from the CSF to the CPe by the Na^+/K^+ ATPase, followed by transport from the CPe to the blood by KCC3 and perhaps KCC1 and as yet unidentified basolateral K^+ channels (3). However, although K^+ must be removed from the CSF by apical CPe uptake followed by basolateral efflux, some K^+ ions must also be returned to the CSF to prevent hypokalorrhachia (low CSF $[K^+]$), and the most likely conduits for this are the apical K^+ channels (3). It is possible that KCNE2-containing channels are required for regulating CSF $[K^+]$ when it has been acutely perturbed; furthermore, we only measured the $[K^+]$ of cisternal CSF for accessibility reasons, but it is possible that the $[K^+]$ of other, inaccessible CSF fractions is regulated by CPe KCNE2-containing channels.

These caveats notwithstanding, we hypothesize two functions for KCNQ1-KCNE2 and/or KCNA3-KCNE2 in the CPe. First, they may provide a K^+ efflux pathway to counteract K^+ influx through the apical Na^+/K^+ ATPase, somewhat analogous to the role of KCNQ1-KCNE2 coupled to the gastric H^+/K^+-ATPase in parietal cells. Second, KCNQ1-KCNE2 and KCNA3-KCNE2 may regulate Cl^- secretion from the CPe to the CSF, as does the related KCNQ1-KCNE3 channel in the colon (26). In support of this hypothesis, we found that *Kcne2* deletion increased outward K^+ current, hyperpolarized the CPe, and increased CSF $[Cl^-]$. The hyperpolarization would tend to drive out Cl^- ions *via* apical channels such as the as-yet unidentified apical anion channel, tallying well with the increased CSF $[Cl^-]$ in *Kcne2*$^{-/-}$ mice (Table 1; Fig. 6*J*).

KCNQ1 is recognized primarily for its roles in the heart and polarized epithelia outside the CNS, although it was recently reportedly to be detected in forebrain neuronal networks and brainstem nuclei, where its precise function has not yet been ascertained (27). Mice with an LQTS-associated KCNQ1 variant knocked-in were found to have seizure-precipitated cardiac arrhythmic episodes, suggesting a

E) Merged, magnified view of adult *Kcne2*$^{+/+}$ mouse CPe images from *D*, showing strong overlap of Kcnq1 (Q1, red) and NKCC1 (NK, green), giving yellow signal. Representative of $n = 2$ tissue sections. *F*) Immunofluorescence of adult *Kcne2*$^{-/-}$ mouse CPe, showing lack of colocalization of Kcnq1 (Q1, red) with the apically localized NKCC1 (NK, green). Yellow arrowhead, punctate Kcnq1 staining; blue arrowhead, diffuse Kcnq1 staining. Representative of $n = 3$ tissue sections. *G*) Immunofluorescence of adult *Kcne2*$^{+/+}$ mouse CPe, showing colocalization of Kcne2 (E2, red) with Kcna3 (A3; green); DAPI staining (blue). Representative of $n = 3$ tissue sections. *H*) Immunofluorescence of adult *Kcne2*$^{+/+}$ mouse CPe, showing colocalization of NKCC1 (NK, green) with Kcna3 (A3; red) (white arrow). Representative of $n = 2$ tissue sections. *I*) Immunofluorescence of adult *Kcne2*$^{-/-}$ mouse CPE, showing lack of colocalization of Kcna3 (A3, red) with the apically localized NKCC1 (NK, green); DAPI staining (D, blue). Representative of $n = 3$ tissue sections. *J*) Model suggesting the effect of *Kcne2* deletion in the CPe. Kcne2 deletion increases currents though Kcnq1 and Kcna3 and switches them to the basolateral membrane. Increased K^+ currents hyperpolarize the cell, possibly increasing Cl^- efflux through apical anion channels (AC). KCC, K^+/Cl^- cotransporter; NKA, Na^+/K^+-ATPase; NKCC, NKCC1. Scale bars = 50 μm (*A*, *B*); 10 μm (*C*, *F*); 200 μm (*D*); 40 μm (*E*, *I*); 3 μm (*G*, *H*).

role for KCNQ1 in regulating neuronal excitability, and also a potential mechanistic basis for sudden unexplained death in epilepsy in humans (27). A role for KCNQ1 in regulating CSF composition, as we report here, raises questions as to whether this magnitude of altered CSF composition could also contribute to neuronal excitability disorders, for example, by shifting the resting membrane potential of the neurons or glial cells which it bathes. It also raises the issue of whether CPe KCNQ1-KCNE2 channels, despite the importance of KCNQ1 to human cardiac function, can ever constitute a therapeutic target for treating disorders of the nervous system involving deregulated CSF secretion and composition, including cerebral edema and intracranial hypertension. Although KCNQ1-KCNE1 channels are important for human ventricular myocyte repolarization and their loss of function linked to LQTS, KCNQ1-KCNE2 channels have a different pharmacological profile than KCNQ1-KCNE1 channels, including increased sensitivity to the Chromanol 293B-like molecule IKs124 (28). In addition, KCNQ1 agonists, which could potentially be used to hyperpolarize the CPe, would not necessarily be cardiotoxic as they would not be predicted to prolong the QT interval.

The recent discovery of a human *KCNE2* mutation in a case of neonatal seizures was intriguing and, if supported by further similar findings, could suggest a role in human inherited epilepsy (10), although how disruption of the function of KCNE2 in the CPe membrane might potentially alter neuronal excitability remains unclear. Targeted deletion of the *Slc4a10* gene, which encodes the Na^+-coupled Cl^--HCO_3^- exchanger Slc4a10, expressed on the CPe basolateral membrane, decreases seizure susceptibility and decreases basolateral Cl^- efflux; however, perturbations in CSF pH appeared more important in the decreased neuronal excitability in this case (29), whereas we did not observe changes in CSF pH with *Kcne2* deletion (Table 1). It is important to note that although we have focused on the roles of KCNE2 in the CPe because of its prominent expression there compared with that in the rest of the brain, the previous discoveries that KCNE2 regulates KCNQ2-KCNQ3 and HCN (pacemaker) channels *in vitro* and that their neuronal expression potentially overlaps, for example, in the thalamus and hippocampus (13, 30, 31), suggest that KCNE2 could also play significant roles directly in specific neurons. FJ

The authors are grateful for expert assistance from K. La Perle, L. Cohen-Gould (Director of the Electron Microscopy and Histology Core Facility at Weill Cornell Medical College), M. S. Jiao, and the Molecular Cytology Core Facility of Memorial Sloan-Kettering Cancer Center. The authors thank Antonio Felipe (Universitat de Barcelona, Barcelona, Spain), Neil Harrison (Columbia University, New York, NY, USA), and Charles Inturrisi (Weill Cornell Medical College, New York, NY, USA) for advice, reagents, and other resources. This work was supported by the U.S. National Heart, Lung, and Blood Institute, National Institutes of Health (NIH; R01-HL079275), the American Heart Association (grant-in-aid 0855756D), and an Irma T. Hirschl Career Scientist Award (to G.W.A.). K.P. was supported by an NIH predoctoral training grant (T32-GM073546).

REFERENCES

1. Lindvall-Axelsson, M., Hedner, P., and Owman, C. (1989) Corticosteroid action on choroid plexus: reduction in Na^+-K^+-ATPase activity, choline transport capacity, and rate of CSF formation. *Exp. Brain Res.* **77,** 605–610
2. Serot, J. M., Bene, M. C., and Faure, G. C. (2003) Choroid plexus, aging of the brain, and Alzheimer's disease. *Front. Biosci.* **8,** s515–521
3. Millar, I. D., Bruce, J., and Brown, P. D. (2007) Ion channel diversity, channel expression and function in the choroid plexuses. *Cerebrospinal Fluid Res.* **4,** 8
4. Speake, T., Kibble, J. D., and Brown, P. D. (2004) Kv1.1 and Kv1.3 channels contribute to the delayed-rectifying K^+ conductance in rat choroid plexus epithelial cells. *Am. J. Physiol. Cell Physiol.* **286,** C611–620
5. Verma-Kurvari, S., Border, B., and Joho, R. H. (1997) Regional and cellular expression patterns of four K^+ channel mRNAs in the adult rat brain. *Brain Res. Mol. Brain Res.* **46,** 54–62
6. Ames, A., 3rd, Higashi, K., and Nesbett, F. B. (1965) Relation of potassium concentration in choroid plexus fluid to that in plasma. *J. Physiol.* **181,** 506–515
7. McCrossan, Z. A., and Abbott, G. W. (2004) The MinK-related peptides. *Neuropharmacology* **47,** 787–821
8. Abbott, G. W., Sesti, F., Splawski, I., Buck, M. E., Lehmann, M. H., Timothy, K. W., Keating, M. T., and Goldstein, S. A. (1999) MiRP1 forms I_{Kr} potassium channels with HERG and is associated with cardiac arrhythmia. *Cell* **97,** 175–187
9. Sesti, F., Abbott, G. W., Wei, J., Murray, K. T., Saksena, S., Schwartz, P. J., Priori, S. G., Roden, D. M., George, A. L., Jr., and Goldstein, S. A. (2000) A common polymorphism associated with antibiotic-induced cardiac arrhythmia. *Proc. Natl. Acad. Sci. U. S. A.* **97,** 10613–10618
10. Heron, S. E., Hernandez, M., Edwards, C., Edkins, E., Jansen, F. E., Scheffer, I. E., Berkovic, S. F., and Mulley, J. C. (2010) Neonatal seizures and long QT syndrome: a cardiocerebral channelopathy? *Epilepsia* **53,** 293–296
11. Tam, G. W., van de Lagemaat, L. N., Redon, R., Strathdee, K. E., Croning, M. D., Malloy, M. P., Muir, W. J., Pickard, B. S., Deary, I. J., Blackwood, D. H., Carter, N. P., and Grant, S. G. (2010) Confirmed rare copy number variants implicate novel genes in schizophrenia. *Biochem. Soc Trans.* **38,** 445–451
12. Loerch, P. M., Lu, T., Dakin, K. A., Vann, J. M., Isaacs, A., Geula, C., Wang, J., Pan, Y., Gabuzda, D. H., Li, C., Prolla, T. A., and Yankner, B. A. (2008) Evolution of the aging brain transcriptome and synaptic regulation. *PLoS One* **3,** e3329
13. Tinel, N., Diochot, S., Lauritzen, I., Barhanin, J., Lazdunski, M., and Borsotto, M. (2000) M-type KCNQ2-KCNQ3 potassium channels are modulated by the KCNE2 subunit. *FEBS Lett.* **480,** 137–141
14. Hunter, N. L., and Dymecki, S. M. (2007) Molecularly and temporally separable lineages form the hindbrain roof plate and contribute differentially to the choroid plexus. *Development* **134,** 3449–3460
15. Roepke, T. K., Anantharam, A., Kirchhoff, P., Busque, S. M., Young, J. B., Geibel, J. P., Lerner, D. J., and Abbott, G. W. (2006) The KCNE2 potassium channel ancillary subunit is essential for gastric acid secretion. *J. Biol. Chem.* **281,** 23740–23747
16. Roepke, T. K., Kontogeorgis, A., Ovanez, C., Xu, X., Young, J. B., Purtell, K., Goldstein, P. A., Christini, D. J., Peters, N. S., Akar, F. G., Gutstein, D. E., Lerner, D. J., and Abbott, G. W. (2008) Targeted deletion of *kcne2* impairs ventricular repolarization *via* disruption of $I_{K,\,slow1}$ and $I_{to,\,f}$. *FASEB J.* **22,** 3648–3660
17. Liu, L., and Duff, K. (2008) A technique for serial collection of cerebrospinal fluid from the cisterna magna in mouse. *J. Vis. Exp.* **21,** 960
18. Speake, T., Freeman, L. J., and Brown, P. D. (2003) Expression of aquaporin 1 and aquaporin 4 water channels in rat choroid plexus. *Biochim. Biophys. Acta* **1609,** 80–86

19. Roepke, T. K., King, E. C., Reyna-Neyra, A., Paroder, M., Purtell, K., Koba, W., Fine, E., Lerner, D. J., Carrasco, N., and Abbott, G. W. (2009) Kcne2 deletion uncovers its crucial role in thyroid hormone biosynthesis. *Nat. Med.* **15,** 1186–1194
20. Tinel, N., Diochot, S., Borsotto, M., Lazdunski, M., and Barhanin, J. (2000) KCNE2 confers background current characteristics to the cardiac KCNQ1 potassium channel. *EMBO J.* **19,** 6326–6330
21. Sole, L., Roura-Ferrer, M., Perez-Verdaguer, M., Oliveras, A., Calvo, M., Fernandez-Fernandez, J. M., and Felipe, A. (2009) KCNE4 suppresses Kv1.3 currents by modulating trafficking, surface expression and channel gating. *J. Cell Sci.* **122,** 3738–3748
22. Praetorius, J., and Nielsen, S. (2006) Distribution of sodium transporters and aquaporin-1 in the human choroid plexus. *Am. J. Physiol. Cell Physiol.* **291,** C59–C67
23. Lee, M. P., Ravenel, J. D., Hu, R. J., Lustig, L. R., Tomaselli, G., Berger, R. D., Brandenburg, S. A., Litzi, T. J., Bunton, T. E., Limb, C., Francis, H., Gorelikow, M., Gu, H., Washington, K., Argani, P., Goldenring, J. R., Coffey, R. J., and Feinberg, A. P. (2000) Targeted disruption of the Kvlqt1 gene causes deafness and gastric hyperplasia in mice. *J. Clin. Invest.* **106,** 1447–1455
24. Lewis, A., McCrossan, Z. A., and Abbott, G. W. (2004) MinK, MiRP1, and MiRP2 diversify Kv3.1 and Kv3.2 potassium channel gating. *J. Biol. Chem.* **279,** 7884–7892
25. Roepke, T. K., King, E. C., Purtell, K., Kanda, V. A., Lerner, D. J., and Abbott, G. W. (2011) Genetic dissection reveals unexpected influence of β subunits on KCNQ1 K^+ channel polarized trafficking in vivo. *FASEB J.* **25,** 727–736
26. Schroeder, B. C., Waldegger, S., Fehr, S., Bleich, M., Warth, R., Greger, R., and Jentsch, T. J. (2000) A constitutively open potassium channel formed by KCNQ1 and KCNE3. *Nature* **403,** 196–199
27. Goldman, A. M., Glasscock, E., Yoo, J., Chen, T. T., Klassen, T. L., and Noebels, J. L. (2009) Arrhythmia in heart and brain: KCNQ1 mutations link epilepsy and sudden unexplained death. *Sci. Transl. Med.* **1,** 2ra6
28. Heitzmann, D., Grahammer, F., von Hahn, T., Schmitt-Graff, A., Romeo, E., Nitschke, R., Gerlach, U., Lang, H. J., Verrey, F., Barhanin, J., and Warth, R. (2004) Heteromeric KCNE2/KCNQ1 potassium channels in the luminal membrane of gastric parietal cells. *J. Physiol.* **561,** 547–557
29. Jacobs, S., Ruusuvuori, E., Sipila, S. T., Haapanen, A., Damkier, H. H., Kurth, I., Hentschke, M., Schweizer, M., Rudhard, Y., Laatikainen, L. M., Tyynela, J., Praetorius, J., Voipio, J., and Hubner, C. A. (2008) Mice with targeted Slc4a10 gene disruption have small brain ventricles and show reduced neuronal excitability. *Proc. Natl. Acad. Sci. U. S. A.* **105,** 311–316
30. Decher, N., Bundis, F., Vajna, R., and Steinmeyer, K. (2003) KCNE2 modulates current amplitudes and activation kinetics of HCN4: influence of KCNE family members on HCN4 currents. *Pflügers Arch.* **446,** 633–640
31. Yu, H., Wu, J., Potapova, I., Wymore, R. T., Holmes, B., Zuckerman, J., Pan, Z., Wang, H., Shi, W., Robinson, R. B., El-Maghrabi, M. R., Benjamin, W., Dixon, J., McKinnon, D., Cohen, I. S., and Wymore, R. (2001) MinK-related peptide 1: a β subunit for the HCN ion channel subunit family enhances expression and speeds activation. *Circ. Res.* **88,** E84–E87

Received for publication April 21, 2011.
Accepted for publication August 11, 2011.